Applied Surface Science 358 (2015) 556–562

Contents lists available at ScienceDirect

Applied Surface Science

journal homepage: www.elsevier.com/locate/apsusc

Ab initio hybrid DFT calculations of $BaTiO_3$, $PbTiO_3$, $SrZrO_3$ and $PbZrO_3$ (111) surfaces

Roberts I. Eglitis

Institute of Solid State Physics, University of Latvia, 8 Kengaraga Str., Riga LV1063, Latvia

ARTICLE INFO

Article history:
Received 22 April 2015
Received in revised form 22 July 2015
Accepted 3 August 2015
Available online 5 August 2015

Keywords:
Ab initio calculations
(111) surfaces
B3LYP
$BaTiO_3$
$PbTiO_3$
$SrZrO_3$
$PbZrO_3$

ABSTRACT

The results of *ab initio* calculations for polar $BaTiO_3$, $PbTiO_3$, $SrZrO_3$ and $PbZrO_3$ (111) surfaces using the CRYSTAL code are presented. By means of the hybrid B3LYP approach, the surface relaxation has been calculated for two possible B (B = Ti or Zr) or AO_3 (A = Ba, Pb or Sr) $BaTiO_3$, $PbTiO_3$, $SrZrO_3$ and $PbZrO_3$ (111) surface terminations. According to performed B3LYP calculations, all atoms of the first surface layer, for both terminations, relax inwards. The only exception is a small outward relaxation of the PbO_3-terminated $PbTiO_3$ (111) surface upper layer Pb atom. B3LYP calculated surface energies for BaO_3, PbO_3, SrO_3 and PbO_3-terminated $BaTiO_3$, $PbTiO_3$, $SrZrO_3$ and $PbZrO_3$ (111) surfaces are considerably larger than the surface energies for Ti (Zr)-terminated (111) surfaces. Performed B3LYP calculations indicate a considerable increase of Ti—O (Zr—O) chemical bond covalency near the $BaTiO_3$, $PbTiO_3$, $SrZrO_3$ and $PbZrO_3$ (111) surface relative to the $BaTiO_3$, $PbTiO_3$, $SrZrO_3$ and $PbZrO_3$ bulk. Calculated band gaps at the Γ-point near the $PbTiO_3$, $SrZrO_3$ and $PbZrO_3$ (111) surfaces are reduced, but near $BaTiO_3$ (111) surfaces increased, with respect to the $BaTiO_3$, $PbTiO_3$, $SrZrO_3$ and $PbZrO_3$ bulk band gap at the Γ-point values.

1. Introduction

ABO_3 perovskite thin films are important in numerous material research and high technology applications, such as, for example, fuel and hydrogen sensors, non-volatile random access memory devices, as well as microelectronics industry [1,2]. Complementary, the polar $BaTiO_3$, $PbTiO_3$, $SrZrO_3$ and $PbZrO_3$ (111) surfaces are also of fundamental interest. For example, in (001) oriented ABO_3 perovskite films, atoms are stacked simply by neutral BO_2 and AO planes. Just opposite, in polar (111) oriented ABO_3 perovskite thin films, atoms are situated by charged B and AO_3 planes, with drastically different physical and chemical interactions [3].

Motivated by rapidly growing number of high technology applications, a large number of theoretical *ab initio* simulations have been performed for $BaTiO_3$, $PbTiO_3$, $SrZrO_3$ and $PbZrO_3$ (001) and (011) surfaces [4–24]. It is surprising, that despite the high technological potential, only some small number of contributions were reported up to now dealing with $BaTiO_3$, $PbTiO_3$, $SrZrO_3$ and $PbZrO_3$ polar (111) surface *ab initio* calculations [25–28].

From the experimental point of view, antiferroelectric $PbZrO_3$ thin films were grown on $Pt/Ti/SiO_2/Si$ substrates applying predominant (111) orientation with a sol–gel process. The $Pt/PbZrO_3/Pt$ film capacitor exhibited well-saturated hysteresis loops at an applied voltage of 5 V [29]. Sa et al. [30] produced Pr-doped $PbZrO_3$ antiferroelectric thin films on $Pt/Ti/SiO_2/Si$ substrates by a chemical solution deposition method. The $PbZrO_3$ thin films with different Pr doping contents crystallized in perovskite phase with strong (111) preferred orientation. Alkoy et al. [31] produced $PbZrO_3$ thin films on $Pt(111)/Ti/SiO_2/Si$ substrates by sol–gel spin coating. Increasing molarity and thickness led to crystallization and grain growth in the films. Double polarization *vs* electric field hysteresis loops were obtained due to fully [111] pseudo-cubic orientation. Sa et al. [32] proposed a method to improve charge and energy storage performance of $PbZrO_3$ thin films by α-Fe_2O_3 nanoparticles doping. The $PbZrO_3$ thin films were deposited on $Pt(111)/Ti/SiO_2/Si$ substrates. Sa et al. [33] reported the W-doping induced antiferroelectric to ferroelectric phase transition in $PbZrO_3$ thin films prepared on $Pt/Ti/SiO_2/Si$ substrates. With increasing W-doping content, the orientation of the thin films changed from preffered $(111)_{Cubic}$ to complete $(100)_{Cubic}$, due to W-doping induced lattice distortion.

Taking into account the high technological potential of $BaTiO_3$, $PbTiO_3$, $SrZrO_3$ and $PbZrO_3$ surfaces, in this study predictive first-principles calculations of $BaTiO_3$, $PbTiO_3$, $SrZrO_3$ and $PbZrO_3$ polar (111) surface structures were performed. The paper is organized as follows. In Section 2 computational details are presented. The results of simulations for surface structures, charge distributions, energies, and bond populations are reported in Section 3.

E-mail address: rieglitis@gmail.com

http://dx.doi.org/10.1016/j.apsusc.2015.08.010
0169-4332/

Finally, the results are analyzed and conclusions are presented in Section 4.

2. Computational details

First-principles DFT-B3LYP simulations for $BaTiO_3$, $PbTiO_3$, $SrZrO_3$ and $PbZrO_3$ polar (111) surfaces were performed using the CRYSTAL computer code [34]. The main advantage of the CRYSTAL code, important for the study of $BaTiO_3$, $PbTiO_3$, $SrZrO_3$ and $PbZrO_3$ (111) surfaces, is implementation of the isolated 2D slab model. In order to use in calculations the linear combination of atomic orbitals (LCAO)-GTF method, it is desirable to have optimized basis sets (BS). The development of new BSs for $SrTiO_3$, $BaTiO_3$ and $PbTiO_3$ crystals were performed by Piskunov et al. [35]. In presented calculations, this new BS for O atoms, which differs from the early performed calculations [36,37] by inclusion of polarizable *d*-orbitals on O ions, was used. For the Zr atom, in $SrZrO_3$ and $PbZrO_3$ perovskites, the same BS as in Refs. [11,26,38] was used. With aim to perform (111) surface calculations for neutral supercells, 2 electrons have been added to Ba^{2+}, Pb^{2+} and Sr^{2+} ions, 4 electrons to Ba^{4+} and Zr^{4+} ion, and 2 electrons were removed from the O^{2-} ion. Subsequently, all $BaTiO_3$, $PbTiO_3$, $SrZrO_3$ and $PbZrO_3$ polar (111) surface calculations were performed using neutral slabs containing 9 layers and 21 or 24 atoms for B and AO_3-terminations, respectively. Numerical calculations were performed using the hybrid exchange-correlation B3LYP functional including a hybrid of nonlocal Fock exact exchange, LDA exchange and Becke's gradient corrected exchange functional [39], in combination with the nonlocal gradient corrected correlation potential by Lee–Yang–Parr [40]. The reciprocal space integration was performed by sampling the Brillouin zone using the $5 \times 5 \times 1$ extended Pack-Monkhorst net [41].

All $SrZrO_3$, $PbZrO_3$, $BaTiO_3$ and $PbTiO_3$ (111) surfaces have the same symmetry group, and were modeled with two-dimensional slabs, containing nine planes perpendicular to the [111] crystal direction. In order to calculate, for example, polar $SrZrO_3$ (111) surfaces, symmetrical slabs consisting of nine alternating Zr and SrO_3 layers were used (see Fig. 1). One of these slabs is terminated by Zr planes (so called Zr-terminated $SrZrO_3$ (111) surface) and consists of a supercell containing 21 atoms (Zr–SrO_3–Zr–SrO_3–Zr–SrO_3–Zr–SrO_3–Zr) (see Fig. 2a). The second slab is terminated by SrO_3 planes (so called SrO_3-terminated $SrZrO_3$ (111) surface) and consists of a supercell containing 24 atoms (SrO_3–Zr–SrO_3–Zr–SrO_3–Zr–SrO_3–Zr–SrO_3) (see Fig. 2b). These slabs are non-stoichiometric, and they have unit cell formulas $Sr_4Zr_5O_{12}$ and $Sr_5Zr_4O_{15}$, respectively. As it is known from previous computational studies dealing with polar $SrTiO_3$, $BaTiO_3$, $CaTiO_3$, $BaZrO_3$ and $SrZrO_3$ (111) surfaces [25,42–47], a huge

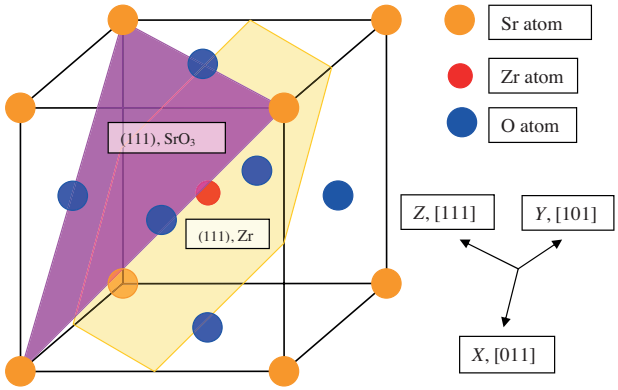

Fig. 1. Sketch of the cubic $SrZrO_3$ perovskite structure showing two possible (111) surface terminations: SrO_3 and Zr.

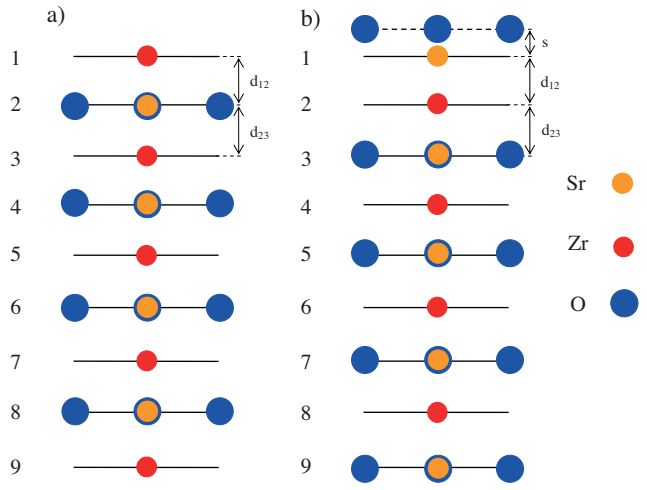

Fig. 2. Sketch of the side views of slab geometries used to study $SrZrO_3$ (111) surfaces. (a) Non-stoichiometric nine-layer slab with Zr-terminated surfaces. (b) Non-stoichiometric nine-layer slab with SrO_3-terminated surfaces with definitions of surface rumpling *s* and the near-surface interplanar separations Δd_{12} and Δd_{23}.

electron redistribution takes place for such terminations in order to cancel the polarity, but the Zr or SrO_3-terminated $SrZrO_3$ (111) surface keeps its insulating character, and therefore such calculations are feasible. Similar model for related $SrZrO_3$ (110) polar surfaces recently was used also by Chen et al. [20]. Their calculation results demonstrated that the charge neutralization and polarity compensation could be achieved by charge redistributions of surface atoms. Of course, it is not feasible to perform calculations for asymmetric stoichiometric slabs with different terminations, for example, Zr–SrO_3–Zr–SrO_3–Zr–SrO_3–Zr–SrO_3, since this would lead to a large dipole moment for an asymmetric slab (see Fig. 3).

Next, the $BaTiO_3$, $PbTiO_3$, $SrZrO_3$ and $PbZrO_3$ cleavage and surface energies were calculated. It is obvious, that $SrZrO_3$ perovskite Zr and SrO_3-terminated (111) surfaces are mutually complementary. (Henceforth, $SrZrO_3$ will be used for presentation purposes, but everything that is said will apply equally also to the $BaTiO_3$, $PbTiO_3$ and $PbZrO_3$ (111) surface energy calculations.) Surfaces with both terminations arise simultaneously under cleavage of the crystal and therefore the relevant cleavage energy is distributed equally between created surfaces. Consequently, the cleavage energy is the same for both terminations. The cleavage energy of

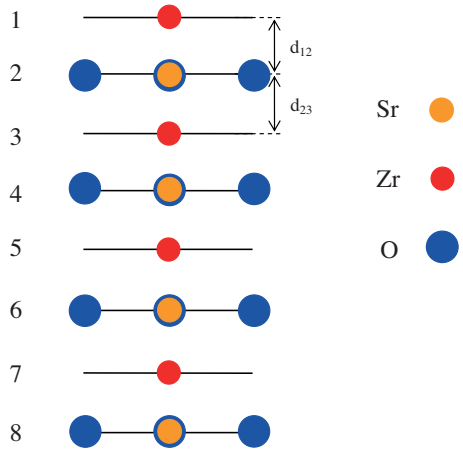

Fig. 3. Sketch of the stoichiometric eight-layer slab with Zr and SrO_3-terminated (111) surfaces with definitions of the near-surface interplanar separations Δd_{12} and Δd_{23}.

Table 1
By means of the hybrid B3LYP method calculated bulk lattice constants (in Å), effective charges Q and bond populations P (in e) of atoms in $BaTiO_3$, $PbTiO_3$, $SrZrO_3$ and $PbZrO_3$ crystals. The experimental bulk lattice constants [48–51] are listed for comparison purposes.

Crystal		$BaTiO_3$	$PbTiO_3$	$SrZrO_3$	$PbZrO_3$
B3LYP calculated lattice const.		4.021	3.963	4.195	4.220
Experimental lattice constant		4.00 [48]	3.97 [49]	4.109 [50]	4.161 [51]
Ion or bond	Property	Value	Value	Value	Value
A	Q	+1.797	+1.392	+1.880	+1.368
B	Q	+2.365	+2.345	+2.174	+2.111
O	Q	−1.387	−1.246	−1.351	−1.160
A—O	P	−0.032	+0.014	+0.002	+0.030
B—O	P	+0.100	+0.100	+0.092	+0.106
O—O	P	−0.038	−0.048	−0.008	−0.020

the complementary $SrZrO_3$ surface $E_{cl}(SrO_3 + Zr)$ can be obtained *via* the following equation:

$$E_{cl}(SrO_3 + Zr) = (1/4)[E_{slab}{}^{unrel}(Zr) + E_{slab}{}^{unrel}(SrO_3) - 9E_{bulk}] \quad (1)$$

where $E_{slab}{}^{unrel}(Zr)$ is the total energy of unrelaxed 21-atom Zr-terminated $SrZrO_3$ slab (see Fig. 2a). $E_{slab}{}^{unrel}(SrO_3)$ is the total energy of unrelaxed 24-atom SrO_3-terminated $SrZrO_3$ (111) slab (see Fig. 2b). E_{bulk} is the bulk energy per formula unit containing 5 atoms in the cubic $SrZrO_3$ structure. Factor 9 in Eq. (1) before the E_{bulk} arises from the fact that 21-atom Zr-terminated and 24-atom SrO_3-terminated $SrZrO_3$ (111) slabs together contain nine 5-atom $SrZrO_3$ bulk unit cells. Factor ¼ means that totally four surfaces are created upon the crystal cleavage.

When both sides of the slab are allowed to relax, the relaxation energies for each of the surfaces can be obtained from the equation:

$$E_{rel}(\chi) = \frac{1}{2}[E_{slab}{}^{rel}(\chi) - E_{slab}{}^{unrel}(\chi)] \quad (2)$$

where χ = Zr or SrO_3 specifies the actual $SrZrO_3$ (111) termination. $E_{slab}{}^{rel}(\chi)$ is the Zr or SrO_3-terminated $SrZrO_3$ (111) slab energy after relaxation. $E_{slab}{}^{unrel}(\chi)$ is the Zr or SrO_3-terminated $SrZrO_3$ (111) slab total energy without the geometry relaxation. Factor ½ means that two surfaces are created upon the crystal cleavage. Finally, the $SrZrO_3$ (111) surface energy is a sum of the cleavage and relaxation energies:

$$E_{surf}(\chi) = E_{cl}(SrO_3 + Zr) + E_{rel}(\chi) \quad (3)$$

3. Numerical results of $BaTiO_3$, $PbTiO_3$, $SrZrO_3$ and $PbZrO_3$ (111) surface calculations

By means of the hybrid B3LYP method the $BaTiO_3$ (4.021 Å), $PbTiO_3$ (3.963 Å), $SrZrO_3$ (4.195 Å) and $PbZrO_3$ (4.220 Å) theoretical bulk lattice constants were calculated. For $BaTiO_3$, $SrZrO_3$ and $PbZrO_3$ they are by 0.53%, 2.09% and 1.42% larger than the corresponding experimental values of 4.00 Å, 4.109 Å and 4.161 Å. In contrast, the B3LYP calculated $PbTiO_3$ bulk lattice constant (3.963 Å) is only by 0.18% smaller than the experimentally detected value of 3.97 Å [48–51] (see Table 1). Thereby, the computational method used in the present calculations is suitable for $BaTiO_3$, $PbTiO_3$, $SrZrO_3$ and $PbZrO_3$ polar (111) surface atomic and electronic structure investigations. The theoretical bulk lattice constants were used in the all following (111) surface investigations.

In order to describe the chemical bonding between different atoms and covalency effects, a classical Mulliken population analysis [52] for the chemical bond populations P and effective charges on atoms Q was used. By means of the hybrid B3LYP functional calculated effective charges for the $BaTiO_3$ crystal bulk are (+2.365e) for the Ti atom, (+1.797e) for the Ba atom, and finally (−1.387e) for the O atom. The bond population value of the chemical bonding between Ti and O atoms in the $BaTiO_3$ crystal is equal to (+0.100e) (see Table 1). The negative chemical bond population value between O and O atoms in the $BaTiO_3$ crystal (−0.038e) indicates repulsion between them. The calculated effective charges for the $PbTiO_3$ bulk are (+2.345e) for the Ti atom, (+1.392e) for the Pb atom, and (−1.246e) for the O atom. The chemical bond population between Ti and O atoms in $PbTiO_3$ is equal to (+0.100e). Finally, the bond population in the $PbTiO_3$ bulk between O and O atoms is negative (−0.048e), namely there are repulsion between O and O atoms.

Table 2
By means of the B3LYP hybrid functional calculated and experimentally measured $BaTiO_3$, $PbTiO_3$, $SrZrO_3$ and $PbZrO_3$ bulk, as well as B and AO_3-terminated (111) surface band gaps at the Γ-point (in electron volts).

Crystal	B3LYP, bulk gap	Exp. bulk gap	B3LYP, B-term.	B3LYP, AO_3-term.
$BaTiO_3$	3.49	3.3 [53]	4.14	3.60
$PbTiO_3$	4.15	3.4 [28]	3.93	3.78
$SrZrO_3$	5.31	5.6 [54]	4.57	4.75
$PbZrO_3$	5.63		3.68	3.95

B3LYP calculated effective Mulliken charges for the Sr atom (+1.880e) are by 6% smaller than the classical ionic charges of (+2e). B3LYP calculated effective charges for the Zr atom (+2.174e) and for the O atom (−1.351e) in the $SrZrO_3$ matrix are obviously smaller than the standard ionic charges of (+4e and −2e) pointing to a large amount of covalency in the chemical bonding between Zr and O atoms. The considerable degree of covalency in the chemical bonding between Zr and O atoms in the $SrZrO_3$ is confirmed also by the large bond population value between Zr and O atoms (+0.092e). The Pb (+1.368e), O (−1.160e) and Zr (+2.111e) effective charges in the $PbZrO_3$ matrix are slightly smaller than in $SrZrO_3$, and consequently the bond population value between Zr and O atoms in the $PbZrO_3$ crystal (+0.106e) is larger than in $SrZrO_3$. The Pb—O bond population (+0.030e) value in the $PbZrO_3$ crystal is exactly 15 times larger than the Sr—O bond population value (+0.002e) in the $SrZrO_3$ matrix.

The calculated by means of the hybrid B3LYP functional bulk band gaps at the Γ-point of four $BaTiO_3$, $PbTiO_3$, $SrZrO_3$ and $PbZrO_3$ perovskites are summarized in Table 2. In the framework of the current paper calculated ABO_3 perovskite bulk band gap is the energy difference (in electron volts) between the top of the valence band and the bottom of the conduction band at the Γ-point. As we can see from Table 2, the $BaTiO_3$ experimentally measured optical band gap is equal to 3.3 eV [53]. The calculated bulk band gap at the Γ-point for the $BaTiO_3$ perovskite 3.49 eV, using the B3LYP functional, is in an excellent agreement with the experimental value. It is worth to notice, that by Sanna et al. [53] by means of the DFT calculated band gap for the $BaTiO_3$ bulk is 1.63 eV, but the DFT + GW band gap amount to 3.68 eV, namely very close to the experimental value and current B3LYP calculation result. The band gap at the Γ-point calculated for $PbTiO_3$ crystal by means of the hybrid B3LYP functional 4.15 eV, is in a satisfactory agreement with the experiment (see Table 2). The discrepancy between the experimental and calculated value is only 22%. This agreement is reasonable, if we take

Table 3
B3LYP calculated relaxation of Ti or Zr, as well as BaO_3, PbO_3 and SrO_3-terminated $BaTiO_3$, $PbTiO_3$, $SrZrO_3$ and $PbZrO_3$ (111) surface upper three layer atoms (as a percentage of the bulk crystal lattice constant a_0 = 4.021, 3.963, 4.195, 4.220 Å, respectively). Positive (negative) values refer to displacements in the direction outwards (inwards) of the surface.

Layer	Ion	$BaTiO_3$ Displ. (Δz) Ti-term. (111)	$PbTiO_3$ Displ. (Δz) Ti-term. (111)	$SrZrO_3$ Displ. (Δz) Zr-term. (111)	$PbZrO_3$ Displ. (Δz) Zr-term. (111)
1	B	−11.19	−7.57	−5.72	−9.24
2	A	−6.22	−10.09	−11.92	+5.92
	O	+2.74	−0.13	+0.79	+2.61
3	B	−0.25	+0.53	+1.53	−2.73

Layer	Ion	$BaTiO_3$ Displ. (Δz) BaO_3-term. (111)	$PbTiO_3$ Displ. (Δz) PbO_3-term. (111)	$SrZrO_3$ Displ. (Δz) SrO_3-term. (111)	$PbZrO_3$ Displ. (Δz) PbO_3-term. (111)
1	A	−1.24	+1.01	−0.74	−0.05
	O	−3.98	−2.52	−0.52	−1.26
2	B	+2.49	+0.02	+0.74	+1.18
3	A	+1.49	+1.26	−0.02	−0.02
	O	−0.25	+1.26	−0.18	−0.02

Table 4
B3LYP calculated surface rumpling s and relative displacements Δd_{ij} between the three near-surface planes, for the B-, and AO_3-terminated $BaTiO_3$, $PbTiO_3$, $SrZrO_3$ and $PbZrO_3$ (111) surfaces. Units are per cent of the bulk lattice constant.

Material	Termination	s	Δd_{12}	Δd_{23}	Termination	Δd_{12}	Δd_{23}
$BaTiO_3$	BaO_3	−2.74	−3.73	+1.00	Ti	−4.97	−5.97
$PbTiO_3$	PbO_3	−3.53	+0.99	−1.24	Ti	+2.52	−10.62
$SrZrO_3$	SrO_3	+0.22	−1.48	+0.76	Zr	+6.20	−13.45
$PbZrO_3$	PbO_3	−1.21	−1.23	+1.20	Zr	−15.16	+8.65

into account the experimental problems in determining the band gap, including the optical absorption edge tails which extend up to several tenths of eV [28]. By means of hybrid B3LYP method calculated band gap at the Γ-point for $SrZrO_3$ bulk (5.31 eV) is in an outstanding agreement with the experimental value of 5.6 eV [54]. Finally, B3LYP calculated band gap at the Γ-point for the $PbZrO_3$ crystal is equal to 5.63 eV (see Table 2).

As follows from the performed hybrid B3LYP calculations for Ti-terminated $BaTiO_3$ (111) surface (see Table 3), the upper layer Ti atom very strongly (by 11.19% of a bulk lattice constant a_0) moves inward. The second layer Ba atom also considerably relaxes inward (by 6.22% of a_0), but just opposite the second layer O atom moves outward by 2.74% of a_0. Finally, inward relaxation of the third layer Ti atom is very small, only 0.25% of a_0. For Ti-terminated $PbTiO_3$ (111) surface all first and second layer atoms moves inward. The strongest relaxation between them exhibit second layer O atom, which moves inward by 10.09% of a_0. The third layer Ti atom relaxes slightly outwards, by 0.53% of a_0. According to the numerical results of performed *ab initio* calculations, the upper layer Zr atoms for Zr-terminated $SrZrO_3$ and $PbZrO_3$ (111) surfaces very strongly (by 5.72% and 9.24% of bulk lattice constant a_0) moves inwards in direction toward the bulk (see Table 3). The second layer Sr and Pb atoms for Zr-terminated $SrZrO_3$ and $PbZrO_3$ (111) surfaces also strongly relaxes, but just in opposite directions by (11.92% of a_0) inwards and by (5.92% of a_0) outwards. The second layer O atoms for both materials relaxes outwards by much smaller displacements than the metal atoms (0.79% and 2.61% of a_0), respectively. Outward and inward relaxation of the third layer metal atoms are smaller than for the first and second layer metal atoms. According to the performed B3LYP calculations, we can see, that the common feature for all four calculated $BaTiO_3$, $PbTiO_3$, $SrZrO_3$ and $PbZrO_3$ perovskites, is rather strong inward relaxation of the upper layer metal atoms (see Table 3).

According to the performed B3LYP calculation results for BaO_3-terminated $BaTiO_3$ (111) surface, both upper layer atoms relax inwards. The upper layer metal atom relaxes inward by 1.24% of a_0, but O atom moves inward even more strongly by 3.98% of a_0 (see Table 3). The second layer Ti atom outward relaxation (2.49% of a_0) is approximately two times larger than the upper layer Ba atom inward relaxation. Finally, the third layer Ba atom rather strongly relaxes outward by 1.49% of a_0, but the same layer O atom relaxes inward by a small magnitude (0.25% of a_0). Just opposite to $BaTiO_3$, $SrZrO_3$ and $PbZrO_3$ perovskites, the PbO_3-terminated $PbTiO_3$ (111) surface upper layer Pb atom slightly relaxes outwards by 1.01% of a_0, while another three perovskite upper layer metal atoms relaxes inwards (see Table 3). For both SrO_3 and PbO_3-terminated $SrZrO_3$ and $PbZrO_3$ polar (111) surfaces all upper layer metal and oxygen atoms moves inwards in direction toward the bulk by relatively small displacement magnitudes ranging from 0.05% of a_0 for the Pb atom on the PbO_3-terminated $PbZrO_3$ (111) surface till 1.26% of a_0 for the O atom on the same surface (see Table 3). The second layer Zr atom outward relaxation magnitude (0.74% of a_0) on the SrO_3-terminated $SrZrO_3$ (111) surface exactly coincides with the first layer Sr atom inward relaxation magnitude (0.74% of a_0). Third layer O atom on the SrO_3-terminated $SrZrO_3$ (111) surface relax inwards by 0.18% of a_0. All another third layer atoms on SrO_3 and PbO_3-terminated $SrZrO_3$ and $PbZrO_3$ (111) surfaces moves inwards by negligibly small displacement, only 0.02% of the lattice constant a_0. According to the performed B3LYP calculations, the common behavior for all four $BaTiO_3$, $PbTiO_3$, $SrZrO_3$, and $PbZrO_3$ perovskites

Table 5
B3LYP calculated cleavage, relaxation, and surface energies for $BaTiO_3$, $PbTiO_3$, $SrZrO_3$ and $PbZrO_3$ (111) surfaces (in electron volts per surface cell).

Surface	Termination	E_{cl}	E_{rel}	E_{surf}
$BaTiO_3$ (111)	Ti-terminated	9.22	−1.94	7.28
	BaO_3-terminated	9.22	−0.82	8.40
$PbTiO_3$ (111)	Ti-terminated	8.31	−2.17	6.14
	PbO_3-terminated	8.31	−0.20	8.11
$SrZrO_3$ (111)	Zr-terminated	9.55	−1.57	7.98
	SrO_3-terminated	9.55	−0.10	9.45
$PbZrO_3$ (111)	Zr-terminated	8.34	−1.41	6.93
	PbO_3-terminated	8.34	−0.13	8.21

Table 6
The A—B bond populations P (in e) and the relevant interatomic distances R (in Å) for two different (111) terminations in $BaTiO_3$, $PbTiO_3$, $SrZrO_3$ and $PbZrO_3$. Symbols I–III denote the number of each plane enumerated from the surface. The nearest-neighbor Ti—O distance in the unrelaxed $BaTiO_3$ bulk lattice is 2.0105 Å, in the unrelaxed $PbTiO_3$ bulk is 1.9815 Å, in the unrelaxed $SrZrO_3$ bulk the nearest Zr—O distance is 2.0975 Å, and finally, in the unrelaxed $PbZrO_3$ bulk the nearest Zr—O distance is equal to 2.11 Å.

Atom A	Atom B	$BaTiO_3$		$PbTiO_3$		$SrZrO_3$		$PbZrO_3$	
		P BaO_3-terminated	R	P PbO_3-terminated	R	P SrO_3-terminated	R	P PbO_3-terminated	R
A(I)	O(I)	−0.022	2.845	+0.050	2.806	+0.004	2.966	+0.050	2.984
B(II)	O(I)	+0.118	1.872	+0.116	1.925	+0.098	2.067	+0.114	2.052
	O(III)	+0.054	2.075	+0.068	2.011	+0.080	2.120	+0.092	2.140
A(III)	B(II)	−0.002	3.496	+0.002	3.416	0.000	3.644	+0.006	3.672
	O(III)	−0.032	2.844	+0.018	2.804	+0.002	2.966	+0.032	2.984
Atom A	Atom B	$BaTiO_3$		$PbTiO_3$		$SrZrO_3$		$PbZrO_3$	
		P Ti-terminated	R	P Ti-terminated	R	P Zr-terminated	R	P Zr-terminated	R
B(I)	A(II)	0.000	3.421	+0.004	3.467	+0.002	3.728	+0.014	3.494
	O(II)	+0.014	1.748	+0.098	1.827	−0.008	1.953	+0.028	1.867
A(II)	O(II)	−0.022	2.866	+0.018	2.830	+0.006	3.014	+0.054	2.987
B(III)	A(II)	0.000	3.410	+0.004	3.316	0.000	3.486	+0.010	3.792
	O(II)	+0.066	2.082	+0.086	1.967	+0.096	2.080	+0.074	2.247

is inward relaxation of all upper layer oxygen atoms, and outward relaxation of the second layer metal atoms (see Table 3).

Experimentally relatively easy measurable properties are the surface rumpling s (the displacement of oxygen with respect to the metal in the upper surface layer) and changes in interlayer distances Δd_{12} and Δd_{23} (1, 2, and 3 are the number of surface layers). My *ab initio* calculation results for this properties are presented in Table 4. The calculations of the interlayer distances are based on the positions of relaxed metal ions. It is possible to see from Table 4, that the BaO_3-terminated $BaTiO_3$ (111) surface shows the reduction of interlayer distance Δd_{12} and expansion of Δd_{23}, whereas, in contrast, the PbO_3-terminated $PbTiO_3$ (111) surface exhibit the expansion of interlayer distance Δd_{12} and reduction of Δd_{23}. In the case of Ti-terminated $BaTiO_3$ and $PbTiO_3$ (111) surfaces, both surfaces exhibit reduction of interlayer distance Δd_{23}. At the same time Ti-terminated $BaTiO_3$ (111) surface shows strong reduction of interlayer distance Δd_{12}, but the Ti-terminated $PbTiO_3$ (111) surface exhibit approximately two time smaller expansion of interlayer distance Δd_{12}. Turning now to $SrZrO_3$ and $PbZrO_3$ perovskites, it is possible to see from Table 4 that both the SrO_3 and PbO_3-terminated $SrZrO_3$ and $PbZrO_3$ (111) polar surfaces exhibits the decrease of interlayer distance Δd_{12} and expansion of Δd_{23}. The Zr-terminated $PbZrO_3$ (111) surface shows the reduction of interlayer distance Δd_{12} and expansion of Δd_{23}, but, just opposite, the Zr-terminated $SrZrO_3$ (111) surface, demonstrate the expansion of the interlayer distance Δd_{12} and reduction of Δd_{23}. My calculated surface rumpling for the PbO_3-terminated $PbZrO_3$ (111) surface is exactly 5.5 times larger than the surface rumpling for the SrO_3-terminated $SrZrO_3$ (111) surface. To the best of my knowledge, there are no experimental measurements for $SrZrO_3$ and $PbZrO_3$ polar (111) surfaces with which I can compare my *ab initio* calculated values of s, Δd_{12} and Δd_{23}.

In the case of (111) surface band gap calculations, the surface states splits off from the top of the valence band and the bottom of the conduction band [55]. The band gap at the Γ-point, namely the energy range with no electronic states between the highest occupied surface state, which split off from the top of the valence band, and lowest unoccupied surface state, which split of from the bottom of the conduction band, were calculated for $BaTiO_3$, $PbTiO_3$, $SrZrO_3$ and $PbZrO_3$ (111) surfaces. The B3LYP calculated band gaps at the Γ-point for the PbO_3 (3.78 eV) and Ti-terminated (3.93 eV) $PbTiO_3$, SrO_3 (4.75 eV) and Zr-terminated (4.57 eV) $SrZrO_3$, as well as for PbO_3 (3.95 eV) and Zr-terminated (3.68 eV) $PbZrO_3$ (111) surfaces, becomes smaller with respect to the calculated bulk band gap at the Γ-point of 4.15 eV for $PbTiO_3$, 5.31 eV for $SrZrO_3$, and 5.63 eV for $PbZrO_3$ (see Table 2). In contrast, the B3LYP calculated band gaps at the Γ-point for the BaO_3 (3.60 eV) and Ti-terminated (4.14 eV) $BaTiO_3$ (111) surfaces are slightly larger than the calculated $BaTiO_3$ bulk band gap at the Γ-point of 3.49 eV. By means of hybrid B3LYP method calculated band gap at the Γ-point for $SrZrO_3$ bulk (5.31 eV) is in an outstanding agreement with the experimental value of 5.6 eV [54]. The narrowest band gap at the Γ-point between all $BaTiO_3$, $PbTiO_3$, $SrZrO_3$ and $PbZrO_3$ (111) surfaces, according to performed B3LYP simulations, is for the BaO_3-terminated $BaTiO_3$ (111) surface (3.60 eV) (see Table 2).

The surface energies for the relaxed $BaTiO_3$, $PbTiO_3$, $SrZrO_3$ and $PbZrO_3$ polar (111) surfaces were calculated using Eqs. (1)–(3). The B3LYP calculated surface relaxation energy for Ti-terminated $BaTiO_3$ (111) surface (−1.94 eV) (see Table 5) is more than two times larger than the corresponding surface relaxation energy for BaO_3-terminated $BaTiO_3$ (111) surface (−0.82 eV). Consequently, the calculated surface energy for Ti-terminated $BaTiO_3$ (111) surface is equal to 7.28 eV, and is 8.40 eV for BaO_3-terminated $BaTiO_3$ (111) surface. The B3LYP calculated Ti-terminated $PbTiO_3$ (111) surface relaxation energy (−2.17 eV) is the largest surface relaxation energy between all calculated $BaTiO_3$, $PbTiO_3$, $SrZrO_3$ and $PbZrO_3$ perovskite (111) surface relaxation energies, and almost eleven times larger than the PbO_3-terminated $PbTiO_3$ (111) surface energy (−0.20 eV) (see Table 5). Consequently, for the $PbTiO_3$ perovskite, there are the largest (111) surface energy difference (1.97 eV) between the Ti-terminated (6.14 eV) and PbO_3-terminated (8.11 eV) (111) surfaces among all four calculated perovskites. My calculated surface energies for SrO_3 and PbO_3-terminated $SrZrO_3$ and $PbZrO_3$ (111) surfaces (9.45 and 8.21 eV, respectively) are much larger than the surface energies for Zr-terminated $SrZrO_3$ and $PbZrO_3$ (111) surfaces (7.98 and 6.93 eV) (see Table 5). The relaxation energies for Zr-terminated $SrZrO_3$ and $PbZrO_3$ polar (111) surfaces are more than fifteen times and more than ten times, respectively, larger than the relaxation energies for SrO_3 and PbO_3-terminated $SrZrO_3$ and $PbZrO_3$ (111) surfaces.

As follows from the chemical bond covalency analysis, for all four calculated $BaTiO_3$, $PbTiO_3$, $SrZrO_3$, and $PbZrO_3$ perovskites, the main effect for the BaO_3, PbO_3, SrO_3 and PbO_3-terminated $BaTiO_3$, $PbTiO_3$, $SrZrO_3$ and $PbZrO_3$ polar (111) surfaces is the strengthening of the Ti—O (Zr—O) chemical bond covalency near the BaO_3 (+0.118e), PbO_3 (+0.116e), SrO_3 (+0.098e), and PbO_3-terminated (+0.114e) $BaTiO_3$, $PbTiO_3$, $SrZrO_3$, and $PbZrO_3$ (111) surfaces (see Table 6).

Table 7
B3LYP calculated Mulliken atomic charges Q (in e) and changes in atomic charges ΔQ with respect to the bulk charges (in e) for the two $BaTiO_3$, $PbTiO_3$, $SrZrO_3$ and $PbZrO_3$ (111) surface terminations. The calculated Mulliken charges in the $BaTiO_3$ bulk are: +2.365e (Ti), −1.387e (O), and +1.797e (Ba). For the $PbTiO_3$ bulk charges are: +2.345e (Ti), −1.246e (O), and +1.392e (Pb). For the $SrZrO_3$ bulk charges are: +2.174e (Zr), −1.351e (O), and +1.880e (Sr). Finally, for the $PbZrO_3$ bulk charges are: +2.111e (Zr), −1.160e (O), and +1.368e (Pb).

Atom, layer	$BaTiO_3$		$PbTiO_3$		$SrZrO_3$		$PbZrO_3$	
	Q BaO_3-terminated	ΔQ	Q PbO_3-terminated	ΔQ	Q SrO_3-terminated	ΔQ	Q PbO_3-terminated	ΔQ
A(I)	+1.792	−0.005	+1.387	−0.005	+1.891	+0.011	+1.400	+0.032
O(I)	−1.054	+0.333	−0.895	+0.351	−1.014	+0.337	−0.848	+0.312
B(II)	+2.313	−0.052	+2.32	−0.025	+2.213	+0.039	+2.157	+0.046
A(III)	+1.784	−0.013	+1.385	−0.007	+1.874	−0.006	+1.324	−0.044
O(III)	−1.326	+0.061	−1.215	+0.031	−1.348	+0.003	−1.139	+0.021
Atom, layer	$BaTiO_3$		$PbTiO_3$		$SrZrO_3$		$PbZrO_3$	
	Q Ti-terminated	ΔQ	Q Ti-terminated	ΔQ	Q Zr-terminated	ΔQ	Q Zr-terminated	ΔQ
B(I)	+1.814	−0.551	+1.771	−0.574	+1.391	−0.783	+1.858	−0.253
A(II)	+1.713	−0.084	+1.171	−0.221	+1.819	−0.061	+0.464	−0.904
O(II)	−1.403	−0.016	−1.258	−0.012	−1.314	+0.037	−1.120	+0.040
B(III)	+2.167	−0.198	+2.200	−0.145	+2.033	−0.141	+2.131	+0.020

This effect, the strong Ti—O (Zr—O) chemical bond covalency, was already well pronounced for $BaTiO_3$, $PbTiO_3$, $SrZrO_3$ and $PbZrO_3$ crystals in the bulk (+0.100e, +0.100e, +0.092e, and +0.106e, respectively). According to performed B3LYP calculations, there are no increase in the Ti—O (Zr—O) chemical bond population value near the Ti (Zr)-terminated $BaTiO_3$, $PbTiO_3$, $SrZrO_3$, and $PbZrO_3$ polar (111) surfaces.

The B3LYP calculated Mulliken effective charges Q, and their changes ΔQ with respect to the bulk values, near the $BaTiO_3$, $PbTiO_3$, $SrZrO_3$, and $PbZrO_3$ (111) surface are presented in Table 7. According to performed B3LYP calculations, the charge of the first layer surface Ti (Zr) atom in the Ti (Zr)-terminated $BaTiO_3$, $PbTiO_3$, $SrZrO_3$, and $PbZrO_3$ polar (111) surfaces is reduced extremely strongly by 0.551e, 0.574e, 0.783e and 0.253e, respectively. Ti (Zr) atoms in the third layer lose much less charge (0.198e, 0.145e and 0.141e) for $BaTiO_3$, $PbTiO_3$ and $SrZrO_3$ perovskites, and even gain a very small amount of charge (0.02e) for $PbZrO_3$ crystal Zr atom. The second layer Ba, Pb and Sr atom charge was reduced by rather small amount of 0.084e, 0.221e and 0.061e, respectively, whereas the second layer Pb charge on $PbZrO_3$ crystal was reduced by a very huge amount of 0.904e. The largest, and almost equal four all four calculated perovskites, charge change on the BaO_3, PbO_3, SrO_3 and PbO_3-terminated $BaTiO_3$, $PbTiO_3$, $SrZrO_3$ and $PbZrO_3$ (111) surfaces is observed for the upper layer O atoms (0.333e, 0.351e, 0.337e and 0.312e, respectively). This gives a large positive change of 0.994e, 1.048e, 1.022e and 0.968e in the charge for each of the BaO_3, PbO_3, SrO_3 and PbO_3-terminated $BaTiO_3$, $PbTiO_3$, $SrZrO_3$ and $PbZrO_3$ (111) surface upper layers. The charge change in the BaO_3, PbO_3, SrO_3 and PbO_3-terminated $BaTiO_3$, $PbTiO_3$, $SrZrO_3$ and $PbZrO_3$ polar (111) surface third layer is negligible in comparison with the upper layer, only 0.17e, 0.086e, 0.003e and 0.019e, respectively.

4. Conclusions

Predictive B3LYP calculations, in order to investigate the polar (111) surface atomic and electronic structure of $BaTiO_3$, $PbTiO_3$, $SrZrO_3$ and $PbZrO_3$ perovskites, were performed. The surface relaxation has been calculated for two possible B (B = Ti or Zr) or AO_3 (A = Ba, Pb or Sr) $BaTiO_3$, $PbTiO_3$, $SrZrO_3$ and $PbZrO_3$ (111) surface terminations. According to performed B3LYP calculations, all atoms of the first surface layer, for both surface terminations and all four investigated perovskites, relax inwards. The only exception is a small outward relaxation of the PbO_3-terminated $PbTiO_3$ (111) surface upper layer Pb atom by 1.01% of the bulk lattice constant a_0. All Ti or Zr-terminated $BaTiO_3$, $PbTiO_3$, $SrZrO_3$ and $PbZrO_3$ (111) surface upper layer atom relaxations are considerably larger than the BaO_3, PbO_3, SrO_3 and PbO_3-terminated (111) surface upper layer atom relaxations. Performed *ab initio* calculation results are in a good agreement with simple chemical bonding theories in assessing surface structure stability [56]. B3LYP calculated bulk band gap at the Γ-point for $BaTiO_3$, $PbTiO_3$ and $SrZrO_3$ perovskites (3.49, 4.15 and 5.31 eV, respectively) is in a good agreement with the experimental values of (3.2, 3.4 and 5.6 eV, respectively). Calculated band gap at the Γ-point for the PbO_3 and SrO_3, as well as Ti and Zr-terminated $PbTiO_3$, $SrZrO_3$ and $PbZrO_3$ polar (111) surfaces, becomes smaller with respect to the bulk band at the Γ-point gap. In contrast, the B3LYP calculated band gap at the Γ-point for BaO_3 and Ti-terminated $BaTiO_3$ polar (111) surface is wider than the $BaTiO_3$ bulk band gap at the Γ-point. B3LYP calculated surface energies for BaO_3, PbO_3, SrO_3 and PbO_3-terminated $BaTiO_3$, $PbTiO_3$, $SrZrO_3$ and $PbZrO_3$ (111) surfaces are considerably larger than the corresponding surface energies for Ti (Zr)-terminated $BaTiO_3$, $PbTiO_3$, $SrZrO_3$ and $PbZrO_3$ (111) surfaces. According to performed *ab initio* calculations, the $BaTiO_3$, $PbTiO_3$, $SrZrO_3$ and $PbZrO_3$ (111) surface energy, for both terminations, is always considerably larger than the earlier calculated respective (011) and (001) surface energy [6,11]. Performed B3LYP calculations indicate a considerable increase of Ti—O (Zr—O) chemical bond covalency near the $BaTiO_3$, $PbTiO_3$, $SrZrO_3$ and $PbZrO_3$ (111) surface (0.118e, 0.116e, 0.098e and 0.114e, respectively) relative to the $BaTiO_3$, $PbTiO_3$, $SrZrO_3$ and $PbZrO_3$ bulk (0.100e, 0.100e, 0.092e and 0.106e, respectively).

Acknowledgements

This work was supported by the Latvian Council of Science Grant No. 374/2012 and ESF Grant No. 2013/0046/1DP/1.1.1.2.0/13/APIA/VIAA/021.

References

[1] M. Dawber, K.M. Rabe, J.F. Scott, Physics of thin-film ferroelectric oxides, Rev. Mod. Phys. 77 (2005) 1083–1130.
[2] J.F. Scott, Ferroelectric Memories, Springer, Berlin, 2000.
[3] R.E. Cohen, Origin of ferroelectricity in perovskite oxides, Nature 358 (1992) 136–138.
[4] J. Padilla, D. Vanderbilt, *Ab initio* study of $BaTiO_3$ surfaces, Phys. Rev. B 56 (1997) 1625–1631.

[5] C. Bungaro, K.M. Rabe, Coexistence of antiferrodistortive and ferroelectric distortions at the $PbTiO_3$ (001) surface, Phys. Rev. B 71 (2005) 035420.
[6] R.I. Eglitis, D. Vanderbilt, *Ab initio* calculations of $BaTiO_3$ and $PbTiO_3$ (001) and (011) surface structures, Phys. Rev. B 76 (2007) 155439.
[7] F. Cora, C.R.A. Catlow, QM investigations on perovskite-structured transition metal oxides: bulk, surfaces and interfaces, Faraday Discuss. 114 (1999) 421–442.
[8] L. Fu, E. Yaschenko, L. Resca, R. Resta, Hartree-Fock studies of surface properties of $BaTiO_3$, Phys. Rev. B 60 (1999) 2697–2703.
[9] Z. Jiang, R. Zhang, D. Wang, D. Sichuga, C.L. Jia, L. Bellaiche, Strain-induced control of domain wall morphology in ultrathin $PbTiO_3$ films, Phys. Rev. B 89 (2014) 214113.
[10] S.I. Lukyanov, A.V. Bandura, R.A. Evarestov, Quantum mechanics based classical molecular dynamics study of water adsorption on (001) $SrMO_3$ surfaces (M = Ti, Zr), Surf. Sci. 611 (2013) 10–24.
[11] R.I. Eglitis, M. Rohlfing, First-principles calculations of the atomic and electronic structure of $SrZrO_3$ and $PbZrO_3$ (001) and (011) surfaces, J. Phys.: Condens. Matter 22 (2010) 415901.
[12] J.L. Wang, G. Tang, X.S. Wu, Thermodynamic stability of $BaTiO_3$ (110) surfaces, Phys. Status Solidi B 249 (2012) 796–800.
[13] B. Meyer, D. Vanderbilt, *Ab initio* study of $BaTiO_3$ and $PbTiO_3$ surfaces in external electric fields, Phys. Rev. B 63 (2001) 205426.
[14] R.I. Eglitis, G. Borstel, E. Heifets, S. Piskunov, E. Kotomin, *Ab initio* calculations of the $BaTiO_3$ (100) and (110) surfaces, J. Electroceram. 16 (2006) 289–292.
[15] Y. Xie, H.T. Yu, G.X. Zhang, H.G. Fu, J.Z. Sun, First-principles investigation of stability and structural properties of the $BaTiO_3$ (110) polar surface, J. Phys. Chem. C 111 (2007) 6343–6349.
[16] G.X. Zhang, Y. Xie, H.T. Yu, H.G. Fu, First-principles calculations of the stability and electronic properties of the $PbTiO_3$ (110) polar surface, J. Comput. Chem. 30 (2009) 1785–1798.
[17] X. Wang, S. Tomoda, T. Shimada, T. Kitamura, Local suppression of ferroelectricity at $PbTiO_3$ surface steps: a density functional theory study, J. Phys.: Condens. Matter 24 (2012) 045903.
[18] E.A. Kotomin, S. Piskunov, Y.F. Zhukovskii, R.I. Eglitis, A. Gopejenko, D.E. Ellis, The electronic properties of an oxygen vacancy at ZrO_2-terminated (001) surfaces of a cubic $PbZrO_3$: computer simulations from the first principles, Phys. Chem. Chem. Phys. 10 (2008) 4258–4263.
[19] T. Shimada, S. Tomoda, T. Kitamura, First-principles study on ferroelectricity at $PbTiO_3$ surface steps, J. Phys.: Condens. Matter 22 (2010) 355901.
[20] H. Chen, Y. Xie, G.H. Zhang, H.T. Yu, A first-principles investigation of the stabilities and electronic properties of $SrZrO_3$ (110) (1×1) polar terminations, J. Phys.: Condens. Matter 26 (2014) 395002.
[21] Y.X. Wang, M. Arai, First-principles study of the (001) surface of cubic $SrZrO_3$, Surf. Sci. 601 (2007) 4092–4096.
[22] R.I. Eglitis, *Ab initio* calculations of $SrTiO_3$, $BaTiO_3$, $PbTiO_3$, $CaTiO_3$ and $BaZrO_3$ (001) and (011) surfaces, Integr. Ferroelectr. 108 (2009) 11–20.
[23] N. Iles, F. Finocchi, F.K.D. Khodja, A systematic study of ideal and double layer reconstructions of ABO_3 (001) surfaces (A = Sr, Ba; B = Ti, Zr) from first principles, J. Phys.: Condens. Matter 22 (2010) 305001.
[24] S. Piskunov, R.I. Eglitis, First principles hybrid DFT calculations of $BaTiO_3/SrTiO_3$ (001) interface, Solid State Ionics 274 (2015) 29–33.
[25] R.I. Eglitis, *Ab initio* calculations of $BaTiO_3$ (111) surfaces, Phase Transit. 86 (2013) 1115–1120.
[26] R.I. Eglitis, *Ab initio* calculations of the atomic and electronic structure of the $SrZrO_3$ (111) surface, Ferroelectrics 436 (2012) 5–11.
[27] Y. Li, R. Yu, T. Shi, Z. Liao, D. Song, H. Zhou, Z. Cheng, J. Zhu, Atomic structure and polarity compensation of $BaTiO_3$ (111) surface, J. Phys.: Condens. Matter 27 (2015) 095901.
[28] R.I. Eglitis, *Ab initio* calculations of $SrTiO_3$, $BaTiO_3$, $PbTiO_3$, $CaTiO_3$, $SrZrO_3$, $PbZrO_3$ and $BaZrO_3$ (001), (011) and (111) surfaces as well as *F* centers, polarons, KTN solid solutions and Nb impurities therein, Int. J. Mod. Phys. B 28 (2014) 1430009.
[29] X.G. Tang, J. Wang, X.X. Wang, H.L.W. Chan, Electrical properties of highly (111)-oriented lead zirconate thin films, Solid State Commun. 130 (2004) 373–377.
[30] T. Sa, N. Qin, G. Yang, D. Bao, Structure and improved electrical properties of Pr-doped $PbZrO_3$ antiferroelectric thin films with (111) preferential orientation, Mater. Chem. Phys. 139 (2013) 511–514.
[31] E.M. Alkoy, S. Alkoy, T. Shiosaki, Investigation of the electrical properties of [111] oriented $PbZrO_3$ thin films obtained by sol–gel process, Jpn. J. Appl. Phys. 45 (2006) 4137–4142.
[32] T. Sa, Z. Cao, Y. Wang, H. Zhu, Enhancement of charge and energy storage in $PbZrO_3$ thin films by local field engineering, Appl. Phys. Lett. 105 (2014) 043902.
[33] T. Sa, N. Qin, G. Yang, D. Bao, W-doping induced antiferroelectric to ferroelectric phase transition in $PbZrO_3$ thin films prepared by chemical solution deposition, Appl. Phys. Lett. 102 (2013) 172906.
[34] V.R. Saunders, R. Dovesi, C. Roetti, M. Causa, N.M. Harrison, R. Orlando, C.M. Zicovich-Wilson, CRYSTAL User Manual, Torino, Italy, University of Torino, 2014.
[35] S. Piskunov, E. Heifets, R.I. Eglitis, G. Borstel, Bulk properties and electronic structure of $SrTiO_3$, $BaTiO_3$, and $PbTiO_3$ perovskites: an *ab initio* HF/DFT study, Comput. Mater. Sci. 29 (2004) 165–178.
[36] E. Heifets, R.I. Eglitis, E.A. Kotomin, J. Maier, G. Borstel, *Ab initio* modeling of surface structure for $SrTiO_3$ perovskite crystals, Phys. Rev. B 64 (2001) 235417.
[37] E.A. Kotomin, R.I. Eglitis, J. Maier, E. Heifets, Calculations of the atomic and electronic structure for $SrTiO_3$ perovskite thin films, Thin Solid Films 400 (2001) 76–80.
[38] R.I. Eglitis, First-principles calculations of $BaZrO_3$ (001) and (011) surface, J. Phys.: Condens. Matter 19 (2007) 356004.
[39] A.D. Becke, Density-functional thermochemistry. III. The role of exact exchange, J. Chem. Phys. 98 (1993) 5648–5652.
[40] C. Lee, W. Yang, R.G. Parr, Development of the Colle-Salvetti correlation-energy formula into a functional of electron density, Phys. Rev. 37 (1988) 785–789.
[41] H.J. Monkhorst, J.D. Pack, Special points for Brillouin-zone integrations, Phys. Rev. B 13 (1976) 5188–5192.
[42] A. Pojani, F. Finocchi, C. Noguera, Polarity on the $SrTiO_3$ (111) and (110) surfaces, Surf. Sci. 442 (1999) 179–198.
[43] A. Pojani, F. Finochi, C. Noguera, A theoretical study of the unreconstructed polar (111) surface of $SrTiO_3$, Appl. Surf. Sci. 142 (1999) 177–181.
[44] W. Liu, C. Wang, J. Cui, Z.Y. Man, *Ab initio* calculations of the $CaTiO_3$ (111) polar surfaces, Solid State Commun. 149 (2009) 1871–1876.
[45] N. Sivadas, H. Dixit, V.R. Cooper, D. Xiao, Thickness-dependent carrier density at the surface of $SrTiO_3$, Phys. Rev. B 89 (2014) 075303.
[46] R.I. Eglitis, *Ab initio* calculations of the atomic and electronic structure of $BaZrO_3$ (111) surfaces, Solid State Ionics 230 (2013) 43–47.
[47] R.I. Eglitis, First-principles calculations of the atomic and electronic structure of $CaTiO_3$. (111) surfaces, Ferroelectrics 424 (2011) 1–6.
[48] K.H. Hellwege, A.M. Hellwege, Ferroelectrics and Related Substances, New Series, vol. 3, Springer Verlag, Berlin, Landolt-Bornstein, 1969.
[49] G. Shirane, R. Pepinsky, B.C. Frazer, X-ray and neutron diffraction study of ferroelectric $PbTiO_3$, Acta Crystallogr. 9 (1956) 131–140.
[50] A.J. Smith, A.R. Welch, Some mixed metal oxides of perovskite structure, Acta Crystallogr. 13 (1960) 653–656.
[51] S. Aoyagi, Y. Kuroiwa, A. Sawada, H. Tanaka, E. Nishibori, M. Takata, M. Sakata, Direct observation of covalency between O and disordered Pb in cubic $PbZrO_3$, J. Phys. Soc. Jpn. 71 (2002) 2353–2356.
[52] C.R.A. Catlow, A.M. Stoneham, Ionicity in Solids, J. Phys. C: Solid State Phys. 16 (1983) 4321–4338.
[53] S. Sanna, C. Thierfelder, S. Wippermann, T.P. Sinha, W.G. Schmidt, Barium titanate ground- and excited-state properties from first-principles calculations, Phys. Rev. B 83 (2011) 054112.
[54] Y.S. Lee, J.S. Lee, T.W. Noh, D.Y. Byun, K.S. Yoo, K. Yamaura, E. Takayama-Muromachi, Systematic trends in the electronic structure parameters of the 4d transition-metal oxides $SrMO_3$ (M = Zr, Mo, Ru and Rh), Phys. Rev. B 67 (2003) 113101.
[55] M. Landmann, E. Rauls, W.G. Schmidt, M.D. Neumann, E. Speiser, N. Esser, GaB *m*-plane: atomic structure, surface bands, and optical properties, Phys. Rev. B 91 (2015) 035302.
[56] J.A. Enterkin, A.E. Becerra-Toledo, K.R. Poeppelmeier, L.D. Marks, A chemical approach to understanding oxide surfaces, Surf. Sci. 606 (2012) 344–355.